PHILOSOPHICAL TRANSACTIONS OF THE ROYAL SOCIETY A MATHEMATICAL, PHYSICAL & ENGINEERING SCIENCES

A Modelling Study of the Mixing of ^{137}Cs in the Seas of the European Continental Shelf

D. Prandle

Phil. Trans. R. Soc. Lond. A 1984 **310**, 407-436
doi: 10.1098/rsta.1984.0002

Phil. Trans. R. Soc. Lond. A **310**, 407–436 (1984) [407]
Printed in Great Britain

A MODELLING STUDY OF THE MIXING OF ^{137}Cs IN THE SEAS OF THE EUROPEAN CONTINENTAL SHELF

By D. PRANDLE

Institute of Oceanographic Sciences, Bidston Observatory, Birkenhead, Merseyside L43 7RA, U.K.

(*Communicated by H. Charnock, F.R.S. – Received 2 August* 1983 – *Revised 3 October* 1983)

CONTENTS

A two-dimensional numerical model is formulated to simulate long-term mixing in the coastal waters over the European Continental Shelf. By using both tidal and wind-driven components, the mean circulation over this region is computed and is shown to be in good agreement with earlier estimates from (i) modelling studies, (ii) observations of residual flow, and (iii) observations of mean sea level distribution. Long-term gradients of sea level in the adjacent oceanic region are found to be unimportant for shelf circulation.

These residual flow components are used to develop a mixing model, observational data of the mixing of ^{137}Cs (released from Windscale over a 17 year period) are used to calibrate and evaluate the model. The model accurately simulates the transport routes of this material both spatially and temporally. This transport is shown to be dependent on both advection and dispersion.

The model is used to determine various time constants for the shelf seas, namely: age, residence times and turn-over-times. Thus, the turn-over-time of the North Sea is calculated to be 530 d compared with a value of 328 d for the Irish Sea. The geographical distribution of turn-over-times differentiates regions of vigorous mixing from more stagnant regions and thereby indicates regions conducive to the formation of thermal fronts. The model also indicates that about one third of the material discharged from Windscale is lost to the ocean in the vicinity of the shelf edge to the north and west of Scotland.

1. Introduction

Caesium 137 (^{137}Cs) has been discharged into the Irish Sea from the Windscale nuclear reprocessing plant at varying rates for about 20 years. The spread of this caesium has been continuously monitored by the Fisheries Radiobiological Laboratory of Lowestoft and by the Deutsches Hydrographisches Institut of Hamburg. Surveys show that the ^{137}Cs leaves the Irish Sea via the North Channel and follows the Scottish Coast around into the North Sea where it is generally dispersed until exiting along the Norwegian Coast. Most of the ^{137}Cs remains in suspension and thus, from an oceanographic viewpoint, the spreading process represents an ideal 'tracer experiment' for developing and evaluating models of long-term circulation. Livingston *et al.* (1982) provide a useful summary of previous studies of the spreading process.

Here we use a two-dimensional (vertically integrated) model of the seas over the Continental Shelf region. By limiting interest to mean conditions over a period of one month or longer, circulation patterns can be constructed by adding separate components resulting from tide, wind etc. This residual circulation model is then used as the basis for a mixing model. The ^{137}Cs survey data are used first to determine the level of 'turbulent' dispersion and subsequently to evaluate the complete model. Having thus established reasonable confidence in the model we calculate various time constants associated with long-term mixing processes and examine the mechanics thereof.

2. Hydrodynamic model

A first step in simulating the spread of ^{137}Cs is to formulate an appropriate hydrodynamic model. This model should reproduce the advective transport of material with an accuracy appropriate to the modelling approach used later for the mixing processes. Presently, the limitations of available computer hardware confine us to the spatial mesh size shown in figure 1, i.e. 20′ of latitude × 30′ of longitude or roughly 35 km square. Ideally a grid size of the order of 1 km should be used. One direct consequence of the coarse grid employed is that interest must be confined to larger scale, longer term mixing processes. In practical terms we hope the model should reasonably simulate mixing in the broad expanse of the North Sea on a month to month basis. Conversely, we cannot expect accurate simulation in smaller regions with irregular topography nor can we expect to reproduce the intense mixing generated by the passage of a single storm.

These limited aims allow the model to be operated with discharge rates from Windscale prescribed on a monthly basis and wind-stress values averaged over three months. (The latter were used simply because of ready availability; monthly-mean wind-stresses would have been

preferable.) Moreover, in the hydrodynamic model we may now confine our requirements to a description of the tidal residual circulation (averaged over a month) and to the 'steady-state' response to (i) wind forcing, (ii) density gradients, and (iii) oceanic pressure gradients. We further confine our interest to the dispersal of any material which is reasonably well-mixed through the water column. (This is true for ^{137}Cs over the Shelf except in some deeper stratified regions (Kautsky *et al.* 1980).) This last condition justifies the use here of a vertically-integrated hydrodynamic model. Clearly such a model will be inaccurate in its simulation of flows in the stratified waters of the Continental Shelf and adjacent oceanic regions.

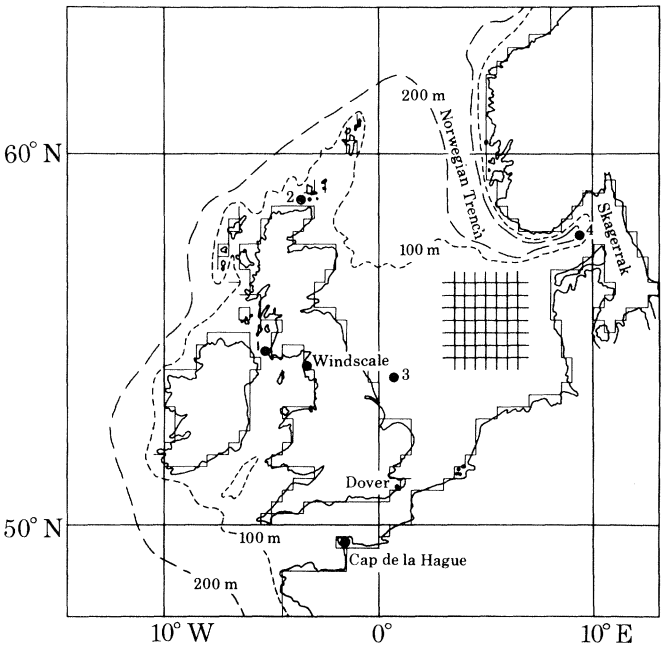

FIGURE 1. The European Continental Shelf. The figure indicates the extent of the numerical model; ●^{3} are locations referred to in figures 7–9.

Figure 1 shows that the boundaries of the present model extend beyond the Shelf edge (effectively delineated by the 200 m contour). This extension is introduced so that dynamically-consistent boundary conditions can be specified along the Shelf edge.

2.1. *Shallow water wave equations*

The equations of motion for the propagation of shallow water waves may be expressed as follows with space coordinates taken along lines of latitude and longitude (Heaps 1969).

$$\frac{\partial u}{\partial t}+u\frac{\partial u}{\partial x}+v\frac{\partial u}{\partial y}+g\frac{\partial z}{\partial x}+\frac{ku(u^2+v^2)^{\frac{1}{2}}}{D+z}-\Omega v = 0, \tag{1}$$

$$\frac{\partial v}{\partial t}+u\frac{\partial v}{\partial x}+v\frac{\partial v}{\partial y}+g\frac{\partial z}{\partial y}+\frac{kv(u^2+v^2)^{\frac{1}{2}}}{D+z}+\Omega u = 0, \tag{2}$$

$$\frac{\partial z}{\partial t}+\frac{\partial}{\partial x}\left\{u(z+D)\right\}+\frac{1}{\Delta x}\frac{\partial}{\partial y}\left\{v(z+D)\,\Delta x\right\} = 0, \tag{3}$$

where u and v are depth-mean velocities along the x- and y-axes respectively; x and y are

orthogonal axes positive to the east and north respectively; Δx is the spacing between lines of longitude; z is the elevation of the water surface above mean sea level; D is the depth of the bed below the same datum; g is gravitational acceleration; t is time; k is the friction coefficient ($= 0.0025$); Ω is the Coriolis parameter ($= 2\omega \sin \phi$), ω is the angular rotation of earth; ϕ is latitude.

2.2. *Tidal model*

The area of interest is represented schematically by the rectangular grid network shown in figure 1. An explicit finite-difference scheme was used to solve the above equations by means of a forward time-stepping procedure with a value for the time step $\Delta t = 72$ s (Prandle 1974). Since we are only concerned with the monthly-mean tidal residual it is sufficient to prescribe only the predominant M_2 constituent along the open-boundary of the model. The requisite M_2 data were supplied by R. A. Flather (I.O.S. Bidston) from his model simulation of tidal propagation in the northeast Atlantic. The results from this latter model were verified by comparison with the extensive observations made by Cartwright *et al.* (1980).

To extract tidal residuals from the model it is essential that cyclic convergence is achieved. Two features were incorporated in the model to encourage this convergence. First, a radiation condition was imposed along the open boundary such that all disturbances at frequencies other than M_2 were assumed to propagate out at the free wave speed (Prandle 1978). Second, horizontal eddy viscosity terms of the form $A\{\partial^2 u/\partial x^2 + \partial^2 u/\partial y^2\}$ and $A\{\partial^2 v/\partial x^2 + \partial^2 v/\partial y^2\}$ were added to the right side of (1) and (2) respectively. The parameter A was made depth dependent, namely $A = 500D$ cm^2 s^{-1}, a format which provides sufficient additional damping in deeper water without significantly influencing propagation in shallower regions (Maier-Reimer (1977) uses a value $A = 2000D$ cm^2 s^{-1}).

Figures 2*a* and *b* show the residual tidal circulation and residual tidal elevations respectively. These results exclude the effect of the convective terms $u\,\partial u/\partial x + v\,\partial u/\partial y$ in (1) and $u\,\partial v/\partial x + v\,\partial v/\partial y$ in (2). Numerical experiments showed that the principal effect of these terms is to add additional structure (i.e. more eddies or gyres) to the residual distributions. However, this additional structure is often exaggerated owing to poor topographic resolution (Zimmerman 1981) and for present purposes was judged to be better neglected.

A further discussion of the results described above follows in §2.5.

2.3. *Wind forcing*

To compute the steady-state response to a uniform surface stress (τ_x, τ_y) we use a linearized version of (1) to (3) namely,

$$\frac{\partial U}{\partial t} + gH\frac{\partial z}{\partial x} + K_{xx}U + K_{xy}V - \Omega V = \frac{\tau_x}{\rho}, \tag{4}$$

$$\frac{\partial V}{\partial t} + gH\frac{\partial z}{\partial y} + K_{xy}U + K_{yy}V + \Omega U = \frac{\tau_y}{\rho}, \tag{5}$$

$$\frac{\partial z}{\partial t} + \frac{\partial U}{\partial x} + \frac{1}{\Delta x}\frac{\partial}{\partial y}\{V\Delta x\} = 0, \tag{6}$$

where $H = D + z$, $U = uH$, $V = vH$, and ρ is the density of sea water.

The linearized friction coefficients K_{xx}, K_{yy} and K_{xy} are calculated from the M_2 tidal velocities (§2.1) with the formulations derived by Heaps (1978). These formulations assume that (i)

the M_2 constituent is predominant, and (ii) the wind-driven velocities are an order of magnitude less than the tidal velocities. The great advantage of this linearized approach is that it enables us to calculate the wind-driven response for any particular month by suitably factoring the responses to unit values of τ_x and τ_y respectively.

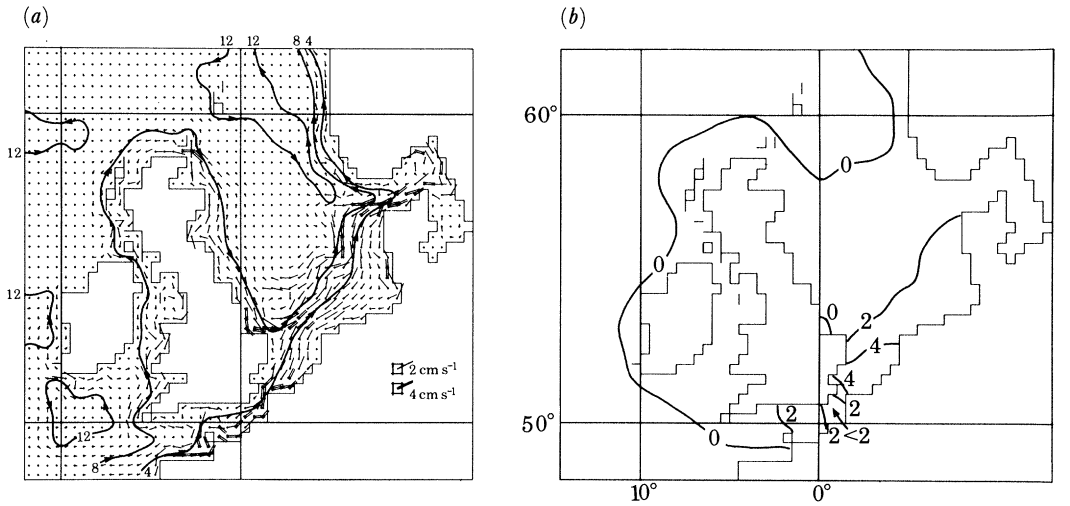

FIGURE 2. Tidal residuals. (*a*) flow: streamlines indicate flow in units of $10^4 \times$ cubic metres per second;

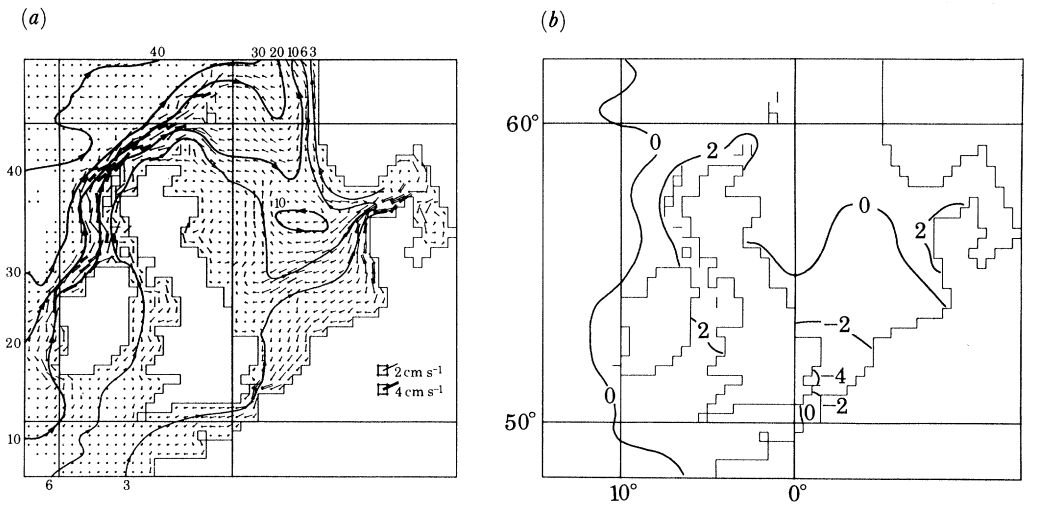

FIGURE 3. Response to a southerly wind ($\tau_y = 0.435$ dyn cm^{-2}). (*a*) flow: streamlines indicate flow in units of $10^4 \times$ cubic metres per second; (*b*) sea level variations in centimetres.

To encourage convergence in the numerical time-stepping solution both the radiation boundary condition and the horizontal eddy viscosity terms described in §2.1 were incorporated in the model. Although the radiation condition introduces a nonlinear element, the model response for the Continental Shelf region remains essentially linear. This holds true because of the siting of the model boundaries in deep water beyond the Shelf edge (see §2.4).

Figures 3*a* and *b* show the response to a steady uniform wind stress $\tau_y = 0.435$ dyn cm^{-2}†

† 1 dyn = 10^{-5} N.

directed from south to north acting over the entire sea region. Likewise, figures 4*a* and *b* show the response to a steady uniform wind stress $\tau_x = 0.529$ dyn cm^{-2} directed from west to east. These values of τ_y and τ_x represent mean values averaged over the period 1951 to 1975 from wind data supplied by K. Thompson of I.O.S. (Bidston). For further details of these wind data see Thompson *et al.* (1983).

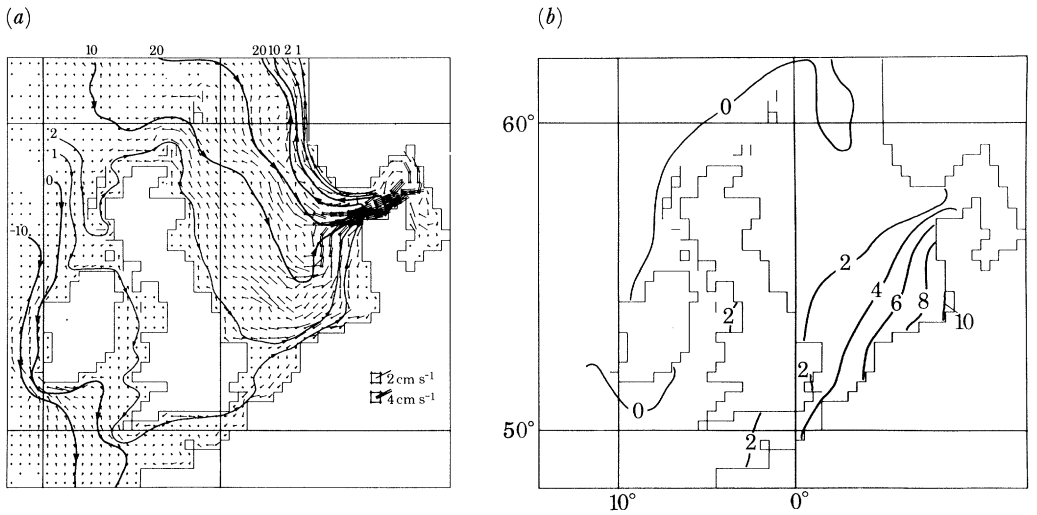

FIGURE 4. Response to a westerly wind ($\tau_x = 0.529$ dyn cm^{-2}). (*a*) flow: streamlines indicate flow in units of $10^4 \times$ cubic metres per second; (*b*) sea level variations in centimetres.

In addition to the temporal averaging noted above these values of (τ_x, τ_y) represent spatial averages over the region 15° W to 5° E and 50° N to 60° N. Spatially varying wind fields were not considered here to avoid further complexity in the later construction of the time series for wind response over a 17 year period. Careful examination of Thompson's data shows that, on average, winds in the western half of this region are about 25% greater than the spatial mean, while in the south-eastern quadrant winds are almost 50% smaller. Overall the departure from the mean value closely approximates a clockwise gyre with a maximum stress around the perimeter of the region of about 30% of the mean value.

A further discussion of the above results follows in §2.5.

2.4. *Response to* (i) *oceanic sea-level gradients, and* (ii) *density gradients*

In addition to prescribing M_2 tidal conditions along the open-sea boundaries of the model, an examination was made of the influence of (i) prescribed mean sea level gradients, and (ii) prescribed steady flows. These additional conditions often produced significant flows in the deeper parts of the model, however the mean flow over the Shelf seas remained sensibly unaffected. Thus, it was concluded that the influence of steady oceanic sea-level gradients (or associated flows) does not extend on to the Continental Shelf and hence, no further consideration of such phenomena is required for the present study. This conclusion, drawn from modelling experiments, has been confirmed theoretically by Wang (1982).

Simulation of the effects of density gradients is limited by the vertically-averaged approach adopted here. However it is possible to incorporate the influence of horizontal density gradients by the inclusion of the terms $(Hg/2\rho)\ \partial\rho/\partial x$ and $(Hg/2\rho)\ \partial\rho/\partial y$ in (4) and (5) respectively.

Mean density distributions for each calendar month were calculated from the temperature and salinity data published by the International Council for the Exploration of the Sea (I.C.E.S. 1970).

Model calculations of the response to these density gradients showed flows generally an order of magnitude less than the values found for tidal or wind forcing. Exceptions were found

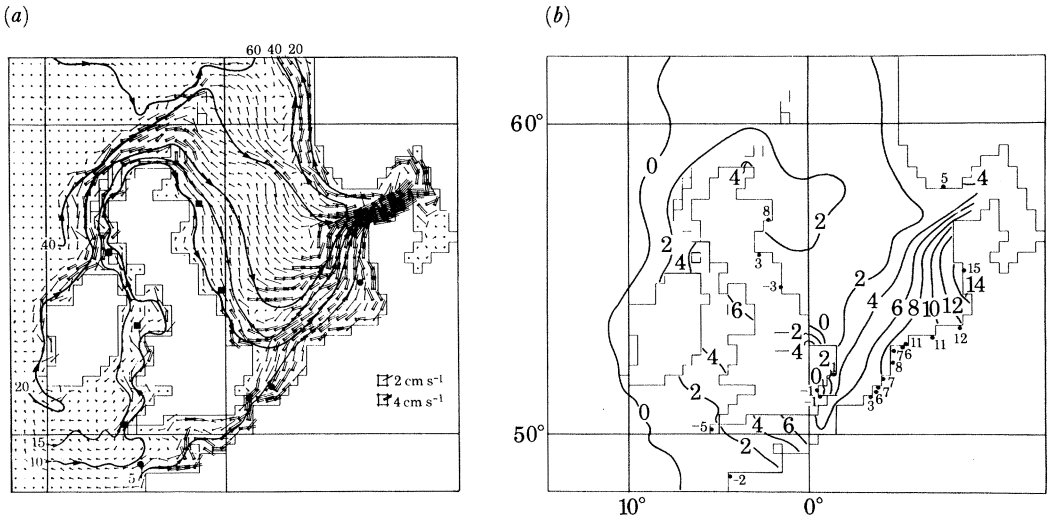

FIGURE 5. Combined response to tidal residual plus mean wind forcing ($\tau_y = 0.435$ dyn cm^{-2}, $\tau_x = 0.529$ dyn cm^{-2}). (*a*) flow: streamlines indicate flow in units of $10^4 \times$ cubic metres per second, ■ – – – ■ indicates distance travelled in 1 year along a streamline path; (*b*) sea level variations in centimetres, ●^{8} is observed variation in mean sea level (Rossiter 1967).

in small localized regions close to major river outflows where significant flows were often indicated. In particular, density gradients in the Skagerrak generated appreciable flows throughout a coastal band of up to 100 km from the Norwegian Coast. However, these localized effects varied considerably from month to month and, on balance, it was decided to omit the effect of density gradients from further consideration. It might be expected that this omission could lead to some deficiency of the flow model in the region of the Norwegian Trench.

2.5. *Mean residual flow*

Perhaps the most surprising feature of figures 2, 3 and 4 is the similarity of the distributions. With a wind blowing from the southwest quadrant, all three residual components (i.e. tidal plus two components of wind) drive water through the English Channel then across the German Bight and finally out of the North Sea via the Norwegian Trench region. Similarly, all three drive water from the north of Scotland in a southeasterly direction to merge with the water from the English Channel in the region of the Skagerrak. The major difference is the response in the Irish Sea where the tidal and southerly wind component drive water northwards whereas the westerly wind component drives water southwards. The similarity in these responses may be attributed to the dominant effect of topography; over the deeper areas the flow appears to be close to a geostrophic balance with consequent topographic steering along the depth contours.

The total time-averaged residual flow pattern (figure 5) shows that maximum residual flows rarely exceed 6 cm s^{-1} except in the Skagerrak. Figure 5*a* shows an estimate of the distances travelled per annum along two particular streamline paths. These show that water originating

off Cornwall would arrive in the Skagerrak in about 5 years time by travelling around the Scottish Coast, or about half that time by travelling more directly through the Dover Strait.

TABLE 1. FLOWS OVER THE EUROPEAN CONTINENTAL SHELF

(Units of flow are $10^4 \times$ cubic metres per second. Positive value indicates flow into the North Sea or northwards through the North Channel.)

	North Channel	Dover Strait	Shetlands to Scotland	Shetlands to Norway	Norwegian Trench
M_2 tidal amplitude	254	102	731	347	133
M_2 residual flow					
(1) present model	3	5	8	−12	−11
(2) Pingree's[6] model	2	3			
(3) other estimate		8[1]			
wind force* of 1 dyn cm^{-2}					
(1) present model	(9, 163°)	(8, 196°)	(39, 215°)	(−46, 212°)	(−66, 221°)
(2) Pingree's model[6]	(10, 140°)	(12, 187°)	(33, 202°)	(−45, 199°)	
(3) other estimate	(10, 160°)[2]	(6, 203°)[1] (8, 204°)[3]			(−31, 300°)[7]
total annual mean flow					
(1) present model	6	9	34	−42	−56
(2) other estimates	5[4] 2.5[5]	16[1]			

Sources: 1, Prandle (1978); 2, Bowden & Hughes (1961); 3, Oerlemans (1978); 4, Howarth (1982); 5, Bowden (1950); 6, Pingree & Griffiths (1980); 7, Davies & Heaps (1980); *, wind stress applied over entire model region, angle indicates the wind direction (relative to North) corresponding to the maximum flow value cited; 1, 3, 6 and 7 provide model data, 1, 2, 4 and 5 provide observational data.

Table 1 quantifies flows through five passages, namely (i) the North Channel of the Irish Sea, (ii) the Dover Strait, (iii) the Fair Isle Channel between Scotland and the Shetlands, (iv) between the Shetlands and Norway, and (v) the Norwegian Trench (across a line approximately 130 km long from (3° W, 61° N) eastwards to the Norwegian coast). In the North Sea we note that the tidal residual flow enters both through the Fair Isle Channel and the Dover Strait (in a ratio 2:1 respectively) and leaves via the Norwegian Trench. A similar pattern follows for the maximum wind response (i.e. with a wind from the south west), but now the Fair Isle Channel contributes five times more than the Dover Strait. At the same time water enters the North Sea in the section between the Norwegian Trench and the Shetlands at a rate approximately half of that entering through the Fair Isle Channel.

We may compare these flow patterns with similar estimates made by Maier-Reimer (1977, 1979) and Pingree & Griffiths (1980). The patterns of both streamlines and mean sea level contours computed by Maier-Reimer are very similar to figures 5*a* and *b*, however, the present response is almost twice as large. The greater magnitude in the present case may be related to the wind data used and in particular to the influence of winds in the Shelf regions outside of the North Sea.

Table 1 compares quantitative values given by Pingree & Griffiths with those presently computed and again good overall agreement is shown. Some additional comparisons with field measurements and other model results are also shown in this table. In general, these comparisons all indicate reasonable agreement.

One interesting discrepancy arises from table 1 concerning the model results of Davies & Heaps (1980). These were obtained from a three-dimensional model of an idealized rectangular basin with dimensions approximating those of the North Sea. Davies & Heaps indicate a wind-

driven flow through the Norwegian Trench equivalent to half the value obtained in the present model and they find a maximum outflow occurs with a wind from the northwest while the maximum outflow in the present model occurs for a southwesterly wind. The aim of the Davies–Heaps study was to demonstrate the influence of the Norwegian Trench. Thus, their model largely neglects both the detailed topography of the North Sea and the influence of the northwestern boundary (where flows generated by winds acting to the west of the North Sea force water through the Fair Isle Channel) and hence this discrepancy is not unexpected.

Davies (1980) carried out a detailed three-dimensional modelling study of wind-driven circulation in the North Sea. He computed the response to a steady wind stress of about 1.5 dyn cm^{-2} directed from just north of southwest (the imposed field included some spatial variability in both magnitude and direction). The computed response for both depth-averaged flow and sea level gradients are in close agreement with the response indicated by figure 4 (i.e. with present model results for a westerly wind). Moreover, Davies compared his results with similar values obtained from a two-dimensional model and again found close agreement. This study by Davies also indicated that the model results were largely insensitive to (i) an improvement in grid resolution by a factor of 3, and (ii) inclusion of the convective terms.

While this agreement between two- and three-dimensional models is encouraging for the approach adopted here, the three-dimensional models clearly indicate significant vertical variation in the wind-driven residual currents. However, in non-stratified regions, mixing through the water column should be sufficiently intense to make the long-term horizontal distribution of material effectively dependent on the vertically-averaged residual current.

As a further check on the validity of the present results, we can compare the mean sea-level distribution shown in figure 5*b* with the distribution obtained by Rossiter (1967). Rossiter's values were obtained from analysing long-term tide gauge recordings and represent the component arising from wind and atmospheric pressure variations. These values are shown in figure 5*b* and clearly agree closely with the model distributions. The sea-level variation computed in this figure includes a tidal contribution, but figure 2*b* indicates that this is a minor component.

3. Mixing model

We now describe the formulation of a mixing model to complement the hydrodynamic model described in the previous section. While numerical modelling of tide and surge propagation has proved to be remarkably successful, mixing models are more troublesome. By way of explanation, we note that while tides represent a well-ordered spectrally narrow phenomenon, mixing can occur over a much wider spectral range and involves random processes.

3.1. *Dispersion equation*

The advective–diffusion equation for turbulent incompressible flow of a conservative substance in two dimensions is (Fischer *et al.* 1979)

$$\frac{\partial c}{\partial t}+u\frac{\partial c}{\partial x}+v\frac{\partial c}{\partial y}=\frac{1}{H}\left\{\frac{\partial}{\partial x}\left(HK_x\frac{\partial c}{\partial x}\right)+\frac{\partial}{\partial y}\left(HK_y\frac{\partial c}{\partial y}\right)\right\}, \tag{7}$$

where c is concentration and K_x, K_y are turbulent diffusion coefficients.

For a radioactive substance that decays with a half-life of period P (7) has an additional term $-0.693c/P$ on the right side (Jefferies *et al.* 1982).

The terms $u\,\partial c/\partial x + v\,\partial c/\partial y$ represent the direct movement of material by the velocity field, i.e. advective transport; while the terms on the right side of (7) represent turbulent diffusion. However, in a numerical model that employs discrete values in space and time any sub-grid scale advection must be accounted for by artificially enhancing the parameters K_x and K_y above their purely diffusive values.

3.2. *Numerical model*

The hydrodynamic model employed a 'Richardson lattice' with z defined at the centre of a grid box and u and v at the mid-points of the orthogonally-oriented grid boundaries. Thus for the grid (x, y) we have $z^{t+\frac{1}{2}}_{x+\frac{1}{2},y+\frac{1}{2}}$, $u^t_{x,y+\frac{1}{2}}$ and $v^t_{x+\frac{1}{2},y}$ where $\frac{1}{2}$ denotes either $\frac{1}{2}\Delta x$, $\frac{1}{2}\Delta y$ or $\frac{1}{2}\Delta t$ giving increments above x, y and t respectively. In the mixing model we define concentration c to be at the centre of a grid box and at the same time level as z.

Making use of (6), equation (7) may be re-written in the form

$$\frac{\partial}{\partial t} Hc + \frac{\partial}{\partial x} Uc + \frac{\partial}{\partial y} Vc = \frac{\partial}{\partial x} HK_x \frac{\partial c}{\partial x} + \frac{\partial}{\partial y} HK_y \frac{\partial c}{\partial y}. \tag{8}$$

This permits the finite-difference approximation for the important advective terms to be written in a conservative form (Roache 1976). Thus (8) is converted to an explicit finite difference formulation as follows:

$$\begin{aligned}[\{Hc\}^{t+\frac{1}{2}}_{x+\frac{1}{2},y+\frac{1}{2}} - \{Hc\}^{t-\frac{1}{2}}_{x+\frac{1}{2},y+\frac{1}{2}}]/\Delta t + \text{advective terms} = \\ [n_1\{K_xH\}^{t-\frac{1}{2}}_{x+1,y+\frac{1}{2}}(c^{t-\frac{1}{2}}_{x+\frac{3}{2},y+\frac{1}{2}} - c^{t-\frac{1}{2}}_{x+\frac{1}{2},y+\frac{1}{2}}) - n_2\{K_xH\}^{t-\frac{1}{2}}_{x,y+\frac{1}{2}}(c^{t-\frac{1}{2}}_{x+\frac{1}{2},y+\frac{1}{2}} - c^{t-\frac{1}{2}}_{x-\frac{1}{2},y+\frac{1}{2}})]/\Delta^2 x \\ + [n_3\{K_yH\}^{t-\frac{1}{2}}_{x+\frac{1}{2},y+1}(c^{t-\frac{1}{2}}_{x+\frac{1}{2},y+\frac{3}{2}} - c^{t-\frac{1}{2}}_{x+\frac{1}{2},y+\frac{1}{2}}) - n_4\{K_yH\}^{t-\frac{1}{2}}_{x+\frac{1}{2},y}(c^{t-\frac{1}{2}}_{x+\frac{1}{2},y+\frac{1}{2}} - c^{t-\frac{1}{2}}_{x+\frac{1}{2},y-\frac{1}{2}})]/\Delta^2 y,\end{aligned} \tag{9}$$

where $n_i = 1$ except at a no-flow boundary where $n_i = 0$.

An upstream differencing approximation was used for the advective terms whereby $\partial Uc/\partial x$ is represented by

$$\{U^t_{x+1,y+\frac{1}{2}}(n_5 c^{t-\frac{1}{2}}_{x+\frac{1}{2},y+\frac{1}{2}} + (1-n_5)\, c^{t-\frac{1}{2}}_{x+\frac{3}{2},y+\frac{1}{2}}) - U^t_{x,y+\frac{1}{2}}(n_6 c^{t-\frac{1}{2}}_{x-\frac{1}{2},y+\frac{1}{2}} + (1-n_6)\, c^{t-\frac{1}{2}}_{x+\frac{1}{2},y+\frac{1}{2}})\}/\Delta x, \tag{10}$$

where

$$n_5 = \begin{cases} 1 & \text{if } U^t_{x+1,y+\frac{1}{2}} > 0, \\ 0 & \text{if } U^t_{x+1,y+\frac{1}{2}} \leqslant 0, \end{cases} \quad \text{and} \quad n_6 = \begin{cases} 1 & \text{if } U^t_{x,y+\frac{1}{2}} > 0, \\ 0 & \text{if } U^t_{x,y+\frac{1}{2}} \leqslant 0, \end{cases}$$

and similarly for $\partial Vc/\partial y$.

A separate model experiment was carried out to test the mass-conservation of the numerical scheme. By omitting the dispersion terms and specifying a uniform discharge from Windscale, mixing was simulated over a 20 year period. A budget was maintained both of losses of material at the open boundaries and of material contained within the model. This budget showed a net loss of only 1% which must be attributed to numerical errors.

An improvement in mass-conservation could be obtained by using the flux-corrected-transport (f.c.t.) technique described by Boris & Book (1973) and by Zalesak (1979). The f.c.t. approach involves a correction to the upstream differencing used for the advective term such that,

$$U_{x+1}c_{x+\frac{1}{2}} - U_x c_{x-\frac{1}{2}}$$

is more accurately represented by

$$\tfrac{1}{2}(U_{x+1}(c_{x+\frac{1}{2}} + c_{x+\frac{3}{2}}) - U_x(c_{x+\frac{1}{2}} + c_{x-\frac{1}{2}})). \tag{11}$$

However this 'correction' must be judiciously applied to avoid introducing instabilities. Using this approach reduced the 1% loss of material cited above to 0.1%. However, the correction more than doubled the time for computation and hence all other results cited refer to the basic numerical scheme shown in (9) and (10).

3.2.1. *Numerical dispersion*

A fundamental problem in the use of low-order difference schemes in mixing problems is the introduction of numerical dispersion. For the difference scheme outlined above, it may be simply shown (Roache 1976) that the magnitude of this numerical dispersion is equivalent to increasing K_x and K_y by K'_x and K'_y respectively where

$$K'_x = \tfrac{1}{2}(u\Delta x - u^2\Delta t); \quad K'_y = \tfrac{1}{2}(v\Delta y - v^2\Delta t). \tag{12}$$

In a simple one-dimensional case stability requires $\Delta x/\Delta t > u$ and hence $\Delta t < \Delta x/u_{\max}$ where $u_{\max}$ is the maximum velocity that may occur. Thus at other locations and times where $u \ll u_{\max}$ and $v \ll v_{\max}$, the major components in (12) are $K'_x = \frac{1}{2}u\Delta x$ and $K'_y = \frac{1}{2}v\Delta y$.

Observed values for K_x and K_y are of the order 5×10^6 cm^2 s^{-1} (see, for example, Bowden 1950). Here we use values of $\Delta x \approx \Delta y \approx 3.5 \times 10^6$ cm and thus for $K'_x < K_x$, $u < 3$ cm s^{-1}. This last criterion shows that by operating the mixing model with the residual velocity field (where on average $u \approx 1$ cm s^{-1}) numerical dispersion may be reduced to an acceptable level. Conversely, in operating the model with instantaneous tidal velocities ($u \approx 50$ cm s^{-1}) numerical dispersion would be excessively large. Moreover, in using only the residual velocity field the values of K_x and K_y must be increased to account for tidal dispersion and hence the relative magnitude of the numerical dispersion is further reduced.

In the simulations described in later sections, the residual velocity field is used with a time step $\Delta t = 12$ h. Additional runs were made to test the sensitivity of the model to changes in Δt. With $\Delta t = 1.2$ h, concentrations were virtually unchanged, thus confirming that the last term in (12) is of little significance.

An alternative method of avoiding excessive numerical dispersion is to use a higher order difference scheme. However with the present grid, several channels are represented schematically by a single mesh point and hence severe boundary condition problems would arise with a higher order scheme.

3.3. *Model evaluation*

A numerical model was formulated with the finite-difference approach indicated above, together with the grid system shown in figure 1 and the residual velocity fields described in § 2. An evaluation of this model is now undertaken, and uses for comparison the spread of ^{137}Cs from Windscale over the period 1964–1980.

In simulating this period, use was made of the following data sets: (i) mean-wind stress values averaged over three-monthly periods (Thompson *et al.* 1983); (ii) mean discharges from Windscale averaged over one monthly periods (Jefferies *et al.* 1982); and (iii) mean discharges from the French reprocessing station at Cap de la Hague averaged over one year periods (Ancellin & Bovard 1980). The time series for the last two data sets are shown in figure 6, discharges from other sources may be safely neglected.

The initial concentration was set to zero throughout the model. In introducing caesium to the model at Windscale (or Cap de la Hague) complete initial mixing was assumed throughout the adjacent grid box. Along the open-boundaries concentrations were set to zero throughout

the simulation period. In reality, there is a background level of ^{137}Cs of about 0.2 picocuries per litre (pCi l^{-1}) (Kautsky *et al.* 1980). To allow for this background level, model concentrations were everywhere increased by the latter amount for the comparisons shown in figures 7–10.

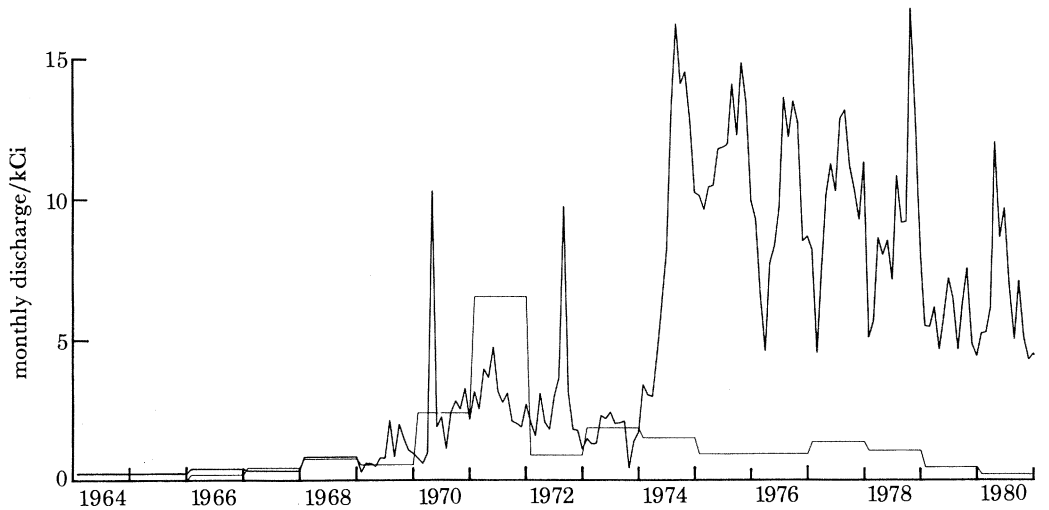

FIGURE 6. Discharge of ^{137}Cs from Windscale (monthly values) and from Cap de la Hague (annual values).

3.3.1. *Determination of dispersion coefficients K_x and K_y*

Preliminary tests showed that values of the dispersion coefficients might be expected to lie in the range 5×10^5 to 5×10^7 cm^2 s^{-1}, at the lower value dispersion was negligible while at the higher value dispersion was clearly excessive. Operating the model with $K_x = K_y = 10^6$ cm^2 s^{-1} produced good agreement between model and observations in the North Sea but computed concentrations were too low in the Irish Sea. Conversely, operating the model with $K_x = K_y = 10^7$ cm^2 s^{-1} produced good agreement in the Irish Sea but low computed concentrations in the North Sea.

Since a major contribution to the dispersion coefficients arises from tidal advection the following formulations for K_x and K_y were finally adopted:

$$K_x = \alpha u_0 R_0; \quad K_y = \alpha v_0 R_0, \tag{13}$$

where u_0 and v_0 are the M_2 current amplitudes and $R_0 = (u_0^2 + v_0^2)^{\frac{1}{2}}$. Other formulations were examined that involved powers of u_0, v_0, residual velocities $\bar{u}$, $\bar{v}$, and the depth H but these showed no clear advantage over (13). For best overall agreement between model and observations a value $\alpha = 1000$ s was used. This is equivalent to the following average values for K_x and K_y (in cm^2 s^{-1}): (i) in the Celtic Sea 1.5×10^6; (ii) in the Irish Sea 6×10^6; (iii) in the English Channel 10×10^6; (iv) in the central and northern North Sea 0.5×10^6; and (v) in the southern North Sea, German Bight and along the English east coast 3×10^6. These values may be compared with the range 5×10^6 to 9×10^6 suggested by Bowden (1950) from analysis of salinity data in the Irish Sea and the value 0.25×10^6 cm^2 s^{-1} used by Maier-Reimer in the North Sea (1977, 1979). In simulating a particular period, (13) could be modified to account for spring-neap variations in tidal amplitude, however this elaboration is not used here.

The significance of a spatial variability in K_x and K_y may be examined by re-writing (7) in the form:

$$\frac{\partial c}{\partial t}+\left\{u-\frac{K_x}{H}\frac{\partial H}{\partial x}-\frac{\partial K_x}{\partial x}\right\}\frac{\partial c}{\partial x}+\left\{v-\frac{K_y}{H}\frac{\partial H}{\partial y}-\frac{\partial K_y}{\partial y}\right\}\frac{\partial c}{\partial y}=K_x\frac{\partial^2 c}{\partial x^2}+K_y\frac{\partial^2 c}{\partial y^2}. \tag{14}$$

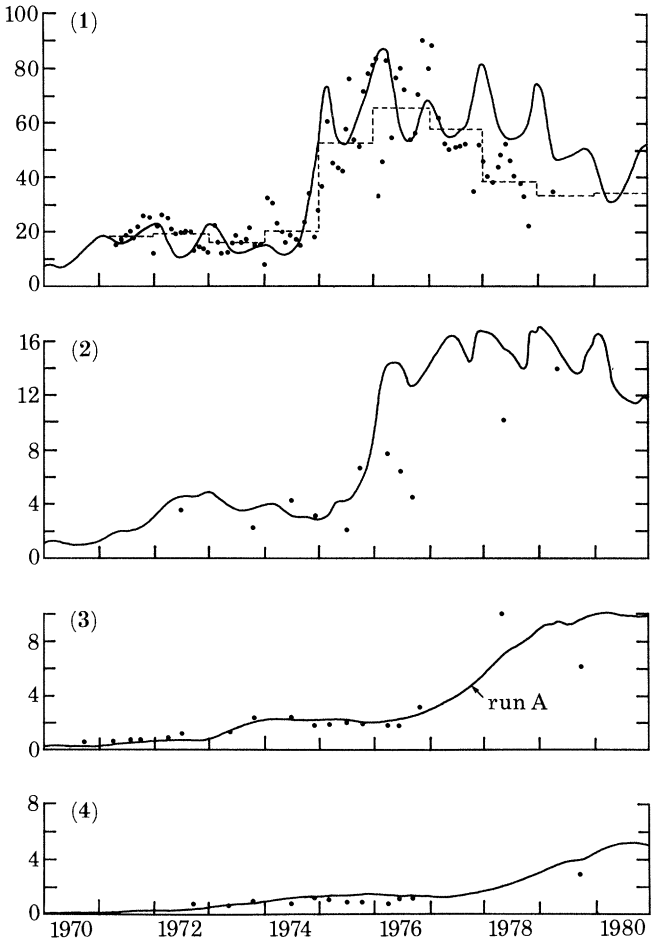

FIGURE 7. Computed against recorded levels of ^{137}Cs (in picocuries per litre) at locations (1) North Channel; (2) Pentland Firth; (3) 54° N, 1° E; (4) Skagerrak, marked in figure 1: ●, observed value; - - - -, observed annual mean value; ——, computed run A, with $\alpha = 1000$ s and three-monthly mean wind stress.

Assuming an average value for K_x or K_y of 3×10^6 cm^2 s^{-1}, noting that $\Delta x \approx \Delta y \approx 3.5\times10^6$ cm, we see that a change in either H or K of 10% between adjacent grid-boxes is equivalent to a residual velocity of about 0.1 cm s^{-1}. Thus, in general, mixing owing to the spatial variability in K_x or K_y will be much less than that from advective transport. However at the shelf edge, where H varies rapidly, topography may significantly enhance mixing by dispersion.

3.3.2. *Computed against recorded distributions of* ^{137}Cs

Figure 7 shows the time histories of computed against recorded concentrations at four locations over the period 1970–1980. The locations chosen are shown in figure 1 and, from the information shown in figure 5, they represent 'travel times' in years from Windscale of approximately, (1) 0.5, (2) 2, (3) 4 and (4) 5. The observational data used here are derived from

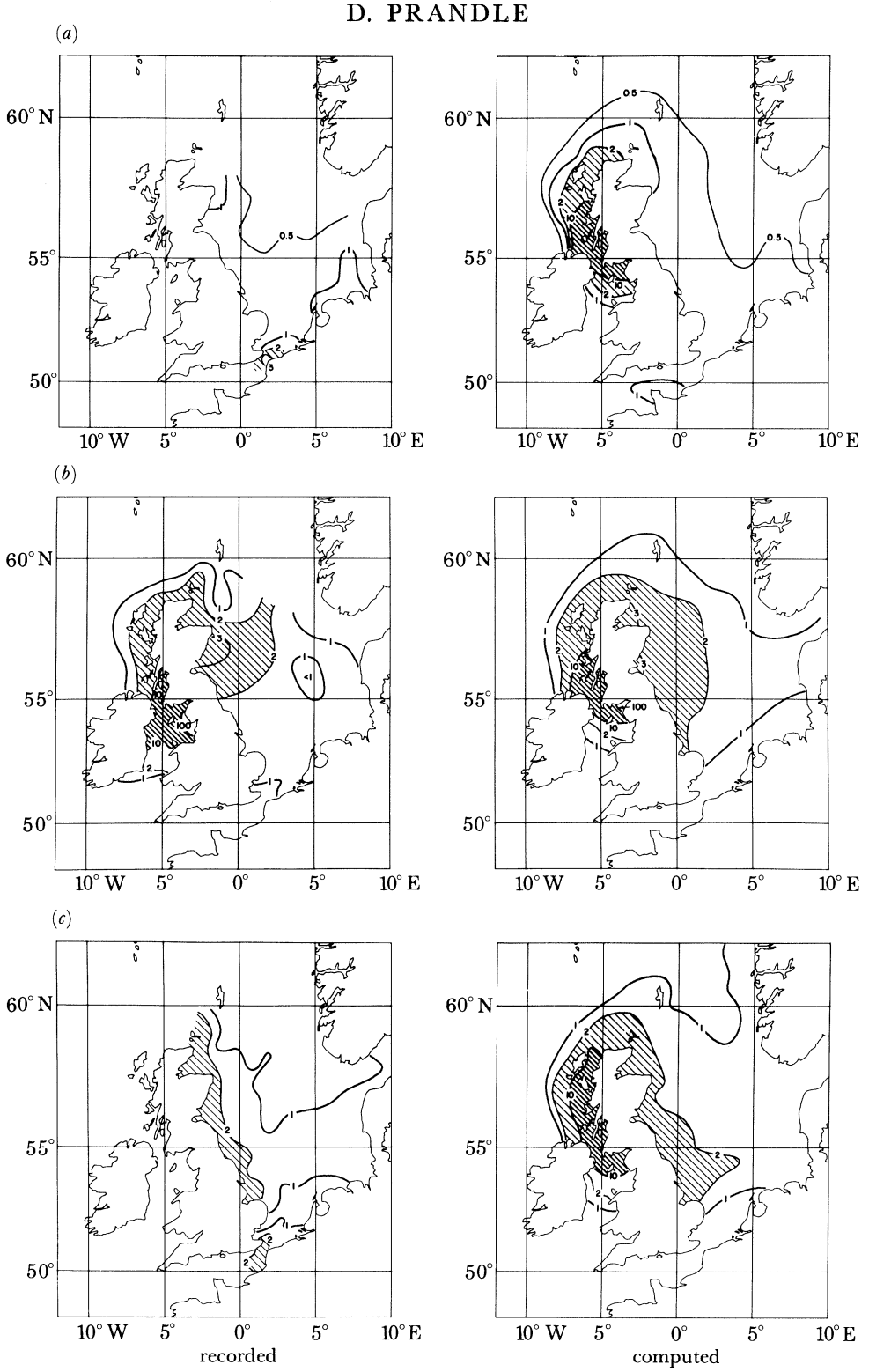

FIGURES 8 *a*, *b*, *c*. For description see opposite.

PHILOSOPHICAL TRANSACTIONS OF THE ROYAL SOCIETY A MATHEMATICAL, PHYSICAL & ENGINEERING SCIENCES

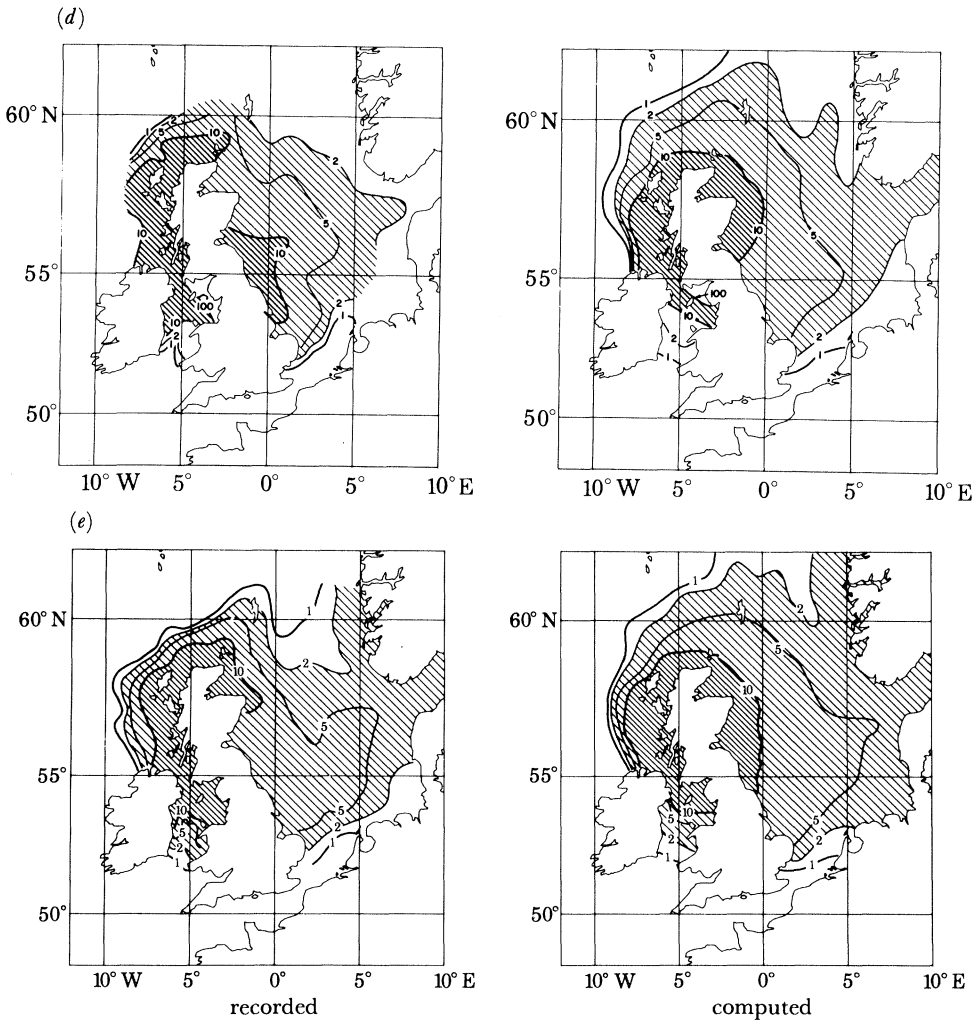

FIGURE 8. Computed against recorded levels of ^{137}Cs (in picocuries per litre): (*a*) March 1971; (*b*) May 1973; (*c*) March 1975; (*d*) May 1978; (*e*) August 1979. (Results for run A.)

Jefferies *et al.* (1982), Kautsky *et al.* (1980), Kautsky (1976) and Lee & Ramster (1981). Additional measurements have been made off the northwestern Scottish coast by McKinley *et al.* (1981) but the complex topography of this region limits the usefulness of these data for present purposes.

(i) *North Channel.* Major peaks shown in the computed results for the North Channel can be readily correlated with peaks in the discharge levels from Windscale (figure 6). However large peaks in the ^{137}Cs concentrations only occur when peak discharges are sustained over 3 or more consecutive months.

There is reasonable agreement in the range of values shown by the model and observations but two clear differences emerge. First, the observations show significantly more high frequency variability. The small response of the model to such frequencies may be attributed to inherent time and spatial averaging with winds averaged over 3 months, inflows averaged over one month and only a single tidal residual component included. Second, model concentrations exceed observations from the middle of 1977 onwards.

In a simple box-model simulation of ^{137}Cs mixing in the Irish Sea and North Channel,

Jefferies *et al.* (1982) found very similar results, i.e. model results agreed well with observations until 1976, after which time model concentrations were significantly higher than observed values. As yet, there is no satisfactory explanation for this divergence but, almost certainly, this divergence originates from within the Irish Sea.

(ii) *Pentland Firth, Central North Sea* (54° N, 1° E) *and Skagerrak.* The general level of agreement at the above three locations is similar to that described earlier, i.e. good in the earlier years but with higher model concentrations in later years. The higher frequency components are progressively damped with increasing distance from Windscale. Over the 11 year period, the mean computed concentrations show dilution ratios of 5, 10 and 20 respectively relative to North Channel concentrations. These dilution rates are in good agreement with observations and indicate the accuracy of the overall simulations.

(iii) *Synoptic distributions.* A major difficulty in the comparisons for specific locations described above arises from the high spatial and temporal gradients in concentration shown in the observed data. This difficulty may be largely overcome by considering synoptic distributions as shown in figure 8.

The component parts of figure 8 show distributions at approximately 2 year intervals over a period of 9 years during which time the peak concentration in the North Sea increased from 1 to 10 pCi l^{-1}. The overall agreement between model and observations is surprisingly good. In particular, the primary transport route for the ^{137}Cs (i.e. around Scotland, across the central North Sea and along the Norwegian coast) is well reproduced both spatially and temporally. This route is directly related to the streamline distributions shown in figures 2–5 and the accuracy of the mixing simulation adds further confidence to these earlier results. The delineation of this route also accords with the deductions of Dooley (1974) and Kautsky *et al.* (1980) where the latter were based solely on ^{137}Cs observations.

Two major deficiencies are evident. First, the poor simulation in the southern North Sea can be attributed to the use of annual-mean discharge rates for the Cap de la Hague releases. Second, the poor simulation in the southern Irish Sea can be attributed to several contributory factors, namely (i) the model assumes complete initial mixing within a grid box at Windscale, (ii) flow resolution is unsatisfactory in this region of complex tidal and residual flow régimes, and (iii) numerical dispersion is significant in this region of highly nonlinear concentration gradients.

3.4. *Sensitivity tests*

The primary aim of the following tests is to establish how the model response varies with changes in the various independent parameters. This procedure reveals not only the robustness of the model but provides an insight into the importance of the various mechanisms involved.

3.4.1. *Variation of K_x with K_y*

Figure 9 shows the time histories of model concentrations at four locations as described for figure 7 but with three differing values for K_x, K_y, namely (i) run C, $\alpha = 0$, (ii) run A, $\alpha = 1000$ s, and (iii) run B, $\alpha = 5000$ s. Run A corresponds to the original optimized model (§3.3.2) and the results for this case lie mid-way between the two alternative formulations. Thus, since run B involves an increase in K_x, K_y by a factor of 5 we conclude that run C involves a decrease (relative to run A) by a similar factor. Hence, this suggests that numerical dispersion, which is isolated in run C, is an order of magnitude less than the dispersion introduced by the optimized values for K_x and K_y.

In the North Channel, increased dispersion decreases the amplitude of the higher frequency variability but has less impact on the mean values. Jefferies *et al.* (1982) estimated that dispersion accounts for between 14–25% of mixing between Windscale and the North Channel.

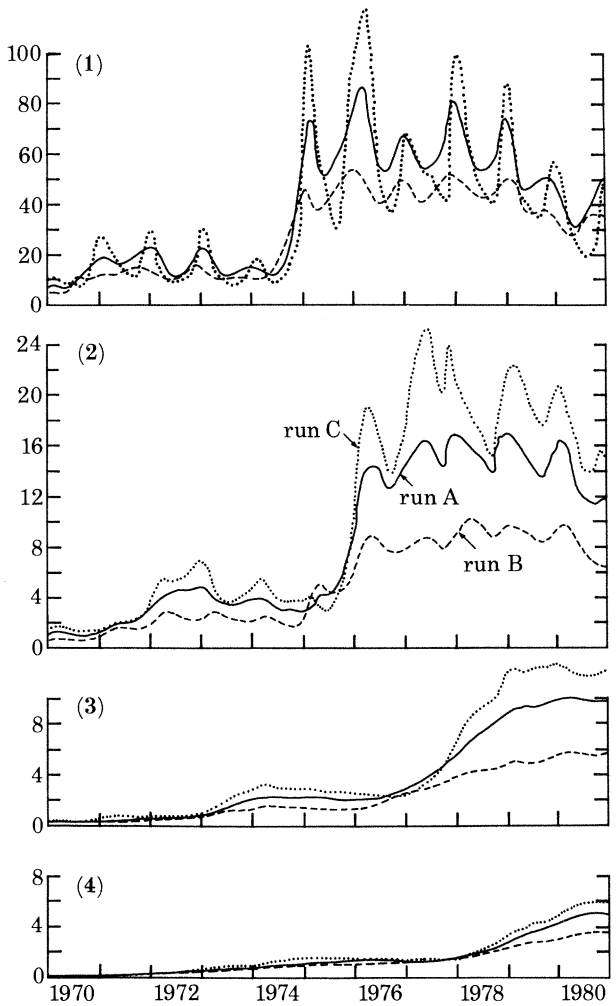

FIGURE 9. Effect of varying the dispersion coefficient on computed values of ^{137}Cs (in picocuries per litre) at locations (1) North Channel; (2) Pentland Firth; (3) 54° N, 1° E; (4) Skagerrak: ——, run A, $\alpha = 1000$ s; – – – –, run B, $\alpha = 5000$ s; . . . . . ., run C, $\alpha = 0$. Three-monthly mean wind stress used throughout.

At greater distances from Windscale, increased dispersion decreases mean concentrations. The concentrations at position 4 are directly related to those at position 3 which suggests that dispersion is insignificant in the intervening region. We might then deduce that advective transport predominates in the central and southern North Sea while dispersive processes are important in the region between the North Channel and the Pentland Firth. Thus, while good agreement between model and observations in the North Sea depends upon the specified values for K_x and K_y, such agreement also requires the correct simulation of advective transport.

PHILOSOPHICAL TRANSACTIONS OF THE ROYAL SOCIETY A MATHEMATICAL, PHYSICAL & ENGINEERING SCIENCES

3.4.2. *Variation of wind forcing*

Figure 10 shows time histories of computed concentrations at four locations; run A corresponds to the case described in §3.3.2. For run D a constant mean wind stress is specified (equal to an average over the years 1951–1975), whereas in run E the wind stress is set to zero. A value of $\alpha = 1000$ s was used in all three runs. A surprising feature of these results is the close agreement for results from run A and run D, this emphasizes that concentrations in the North Sea are primarily determined by a low frequency response to wind forcing.

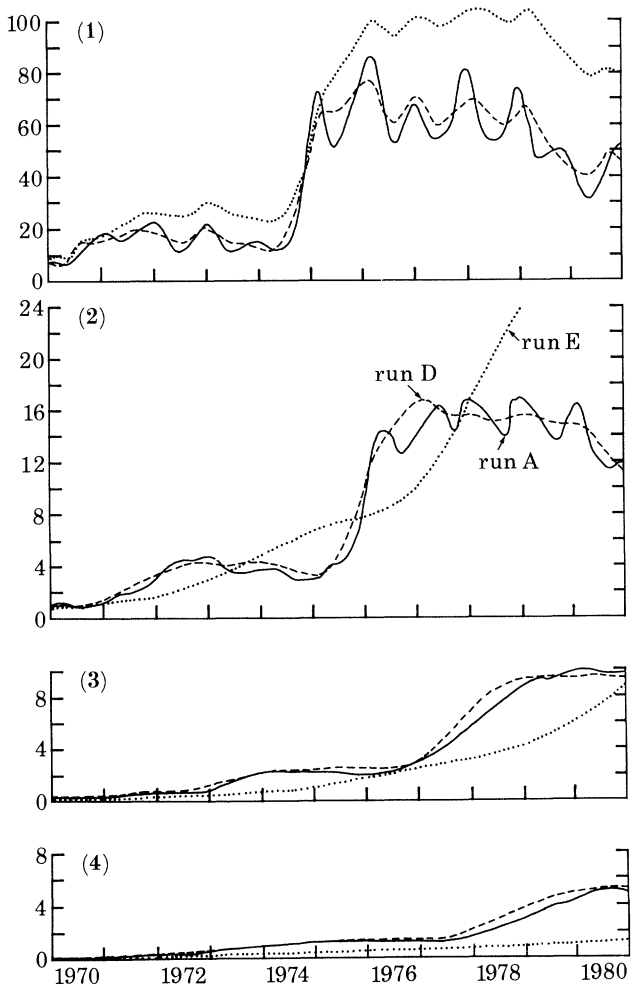

FIGURE 10. Effect of varying the applied wind stress on computed values of ^{137}Cs (in picocuries per litre) at locations (1) North Channel; (2) Pentland Firth; (3) 54° N, 1° E; (4) Skagerrak: ——, run A, wind stress specified as a mean over three months; – – – –, run D, wind stress constant ($\tau_y = 0.435$ dyn cm^{-2}, $\tau_x = 0.529$ dyn cm^{-2}); . . . . . , run E, zero wind stress; $\alpha = 1000$ s used throughout.

By contrast, with zero wind stress, concentrations change by up to a factor of 5 and the time series are radically changed compared with run A. Figures 2–5 show that, on average, wind forcing accounts for about 50 % of the residual circulation. Thus we may deduce that good agreement between model and observed concentrations requires an accurate simulation of the advective transport associated with both long term wind forcing and the residual tidal component.

4. Mixing time-scales

Having developed and validated a model to simulate mixing over the Continental Shelf seas we now use the model to determine various time constants associated with water quality interests. Throughout the section conditions specified in the model correspond to those used in run D (§3.4.2) except where explicitly stated.

4.1. *Time parameters*

The definitions given here are of a simple conceptual nature. More rigorous mathematical definitions are presented in the following section and these largely follow earlier work by Bolin & Rohde (1973) and Zimmerman (1976).

Consider a bounded sea region within which material is introduced at some location (x_0, y_0), then at any position (x, y) within this region we can define:

(i) τ_a 'age' as the time to travel from (x_0, y_0) to (x, y);

(ii) τ_r 'residence time' as the time to travel from (x, y) to the boundary of the region;

(iii) τ_0 'transit time' as the time to travel from (x_0, y_0) to the boundary of the region.

The travel times stated refer to statistical averages. An additional parameter may be defined as

(iv) τ_t 'turn over time' representing the time for the total mass of material originally within a bounded region to be reduced to a factor e^{-1} (i.e. 0.37).

For the simple case of a constant flow, q, through a bounded region of volume V, the average concentration c is given by

$$V\,dc/dt = -qc$$

or

$$c = c_0 e^{-(q/V)t}, \tag{15}$$

where $c = c_0$ when $t = 0$. Hence for $t = \tau_t$

$$c/c_0 = 1/e, \quad t = \tau_t = V/q. \tag{16}$$

Thus for these particular flow conditions the turn-over-time τ_t is equivalent to

(v) τ_f 'flushing time' defined as V/q. (17)

The above five time parameters have been introduced to illustrate their inter-relations. Under certain conditions 'flushing time' and 'turn-over-time' are equivalent, and 'transit time' is merely a particular value for 'residence time'. It will be further shown that the calculation of 'turn-over-time' is analogous to the calculation of 'residence time'. Thus the original five parameters may be reduced to just two basic definitions, namely 'age' and 'residence time'.

4.2. *Calculation of time parameters*

The rate of change of material of concentration c within an area A is given by

$$L(t) = \oint H \frac{dc}{dt}\, dA. \tag{18}$$

The parameters 'age' and 'residence time' both represent centroidal values of the above function but with differing initial and boundary conditions.

(i) *Age* τ_a

Setting initial concentrations to zero throughout the model, a constant rate of inflow of material is introduced and τ_a is given by

$$\tau_a = \int_0^\infty \frac{L(t)}{M}\, t\,\mathrm{d}t, \tag{19}$$

where $M = \oint Hc_\infty \mathrm{d}A$ is the mass of material within the area A at $t \to \infty$. Temporal contributions to τ_a can be described by the normalized function

$$S(t) = L(t)/M. \tag{20}$$

The value of τ_a will vary according to, (i) the location and size of the area A, and (ii) the location of the inflow. By defining A to be a small area surrounding the point (i, j) a 'localized' value $\tau_a(i, j)$ can be obtained. Alternatively, the area A may represent a larger region for which an integrated value $\bar{\tau}_a$ can be determined.

(ii) *Residence time*

Again setting initial concentrations to zero throughout the model, we introduce an initial concentration of material c_i within a small area a surrounding the location (i, j). The value of $\tau_r(i, j)$ for the bounded region of area A is then given by (19) with $M = \oint Hc_i \mathrm{d}a$, i.e. the mass of material originally introduced into the area a. Temporal contributions to τ_r are similarly described by (20) with the last definition for M.

The calculation of 'turn-over-time', τ_t, for any area, a, procedes with the same initial and boundary conditions prescribed in the calculation of τ_r. However, the simulation need only continue until the time t when

$$\oint Hc\mathrm{d}a = M/\mathrm{e}, \tag{21}$$

i.e. until the mass of material contained within the area a is reduced to a fraction e^{-1} of the original mass M. By dividing the left side of (21) by M, the fractional cumulative loss of material from the area a can be illustrated as a continuous function of time.

4.3. *Turn-over time*

Figure 12 shows the fractional loss of material originally evenly dispersed over the North Sea, where that area is defined as the sum of sub-regions 1 to 8 shown in figure 11. Three results are shown to illustrate the sensitivity of τ_t to changes in (*a*) the dispersion coefficient, and (*b*) advective transport. The results for case (i) correspond to the conditions specified for run D (§3.4.2). For case (ii) the value $\alpha = 1000$ s used in the previous case is increased to 5000 s while in case (iii) $\alpha = 1000$ s but the wind-driven residual circulation is set to zero. Curves (i) and (ii) are nearly identical which indicates that the dilution of material initially contained within the North Sea is sensibly independent of dispersion processes (at least within the range of coefficients used). By contrast, curve (iii) indicates a much-reduced dilution rate thereby emphasizing the importance of wind forcing, i.e. of advective transport.

For the three conditions cited above, table 2 indicates values of τ_t for the various sub-regions shown in figure 11 and for some combinations of these sub-regions. The sub-regions were chosen to correspond with the divisions adopted by the International Council for the Exploration of the Sea (I.C.E.S. 1983). In the absence of wind-forcing, regions 1, 2 and 6 in the north-eastern North sea show slow turn-over rates, namely $\tau_t = 1575$, 795 and 733 d respectively,

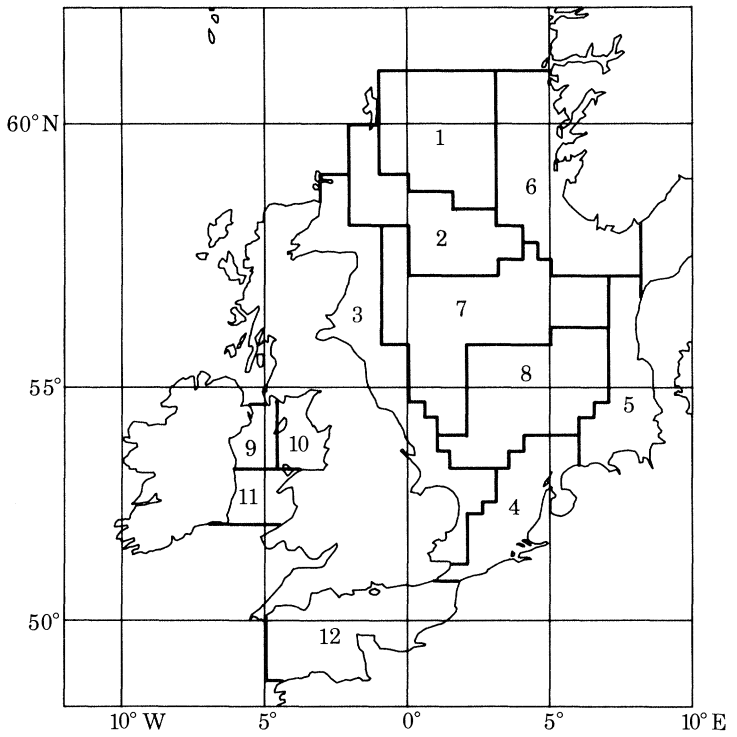

FIGURE 11. Sub-regions of the Continental Shelf (referenced in table 2).

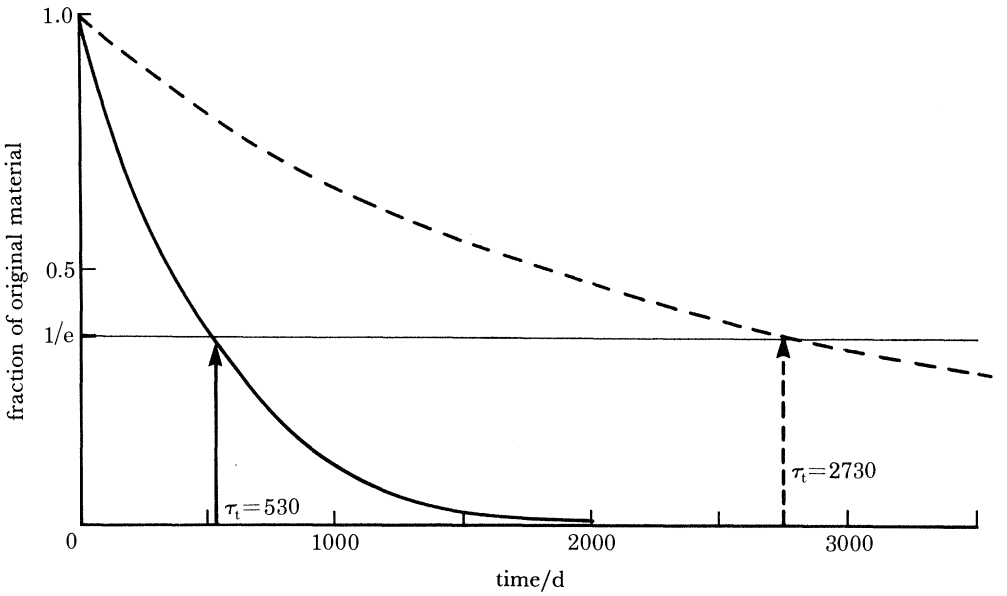

FIGURE 12. Effect of varying (*a*) the dispersion coefficient and (*b*) the applied wind stress on 'turn-over-times' for the North Sea: (i) ——, α = 1000 s, mean wind stress; (ii) (coincides with (i)), α = 5000 s, mean wind stress; (iii) – – – –, α = 1000 s, zero wind stress.

this follows from the small tidal exchange in this area as indicated by table 1. However by including wind-forcing the turn-over times become more rapid, namely τ_t = 177, 156 and 155 d, which indicates the strength of this component in these regions.

Within the North Sea the table shows that values of τ_t can be affected by dispersion but

clearly advective processes predominate, e.g. for area 7, τ_t = 192, 162 and 850 d respectively for cases (i), (ii) and (iii). However in the Irish Sea and English Channel the table suggests that these two mechanisms are more evenly balanced, e.g. for areas 9 and 10 and 11 (Irish Sea) respective values of τ_t are 328, 223 and 518 d while for area 12 (English Channel) respective values of τ_t are 295, 186 and 404 d.

TABLE 2. TURN-OVER-TIMES FOR SUB-REGIONS OF THE SHELF SEAS IN DAYS

area	$K_x = 1000\, u_0 R_0$ $K_y = 1000\, v_0 R_0$ average winds	$K_x = 5000\, u_0 R_0$ $K_y = 5000\, v_0 R_0$ average winds	$K_x = 1000\, u_0 R_0$ $K_y = 1000\, v_0 R_0$ zero winds
1	177	159	1575
2	156	120	795
3	199	109	304
4	78	58	143
5	86	64	258
6	155	154	733
7	192	162	850
8	83	72	175
1+2+3+4+5+6+7+8	530	525	2730
9	92	35	114
10	98	33	145
11	117	39	147
9+10	187	105	304
9+10+11	328	223	518
12	295	186	404
	(i)	(ii)	(iii)

In general, values of τ_t will increase in proportion to a linear dimension of the initial area (see (16)) and this is observed from table 2. Thus, for case (i), the North Sea has a turn-over time of 530 d while for the smaller Irish Sea τ_t = 328 d.

The values for each of the sub-regions 1 to 8 may be compared with the values of τ_f calculated by Davies (1982) for meteorologically induced flow in a hydrodynamic model. A number of differences in approach prevent an exact comparison but for almost every sub-region the present values for τ_t are within a factor of 2 of the values for τ_f given by Davies. Since the latter were calculated from a fully three-dimensional model we may conclude that the use of a vertically integrated model appears to be acceptable for the applications considered here.

Using observed distributions of ^{137}Cs, Jefferies *et al.* (1982) estimated flushing times for sub-regions of the Irish Sea as follows: (9) 240 d; (10) 290 d; (9) and (10) 530 d. These values exceed present estimates by a factor of about 2.5. Reasons for the deficiency of the model in this area have been discussed in §3.3.2; clearly the assumption of complete initial mixing within the selected regions significantly reduces present estimates of τ_t.

Returning to the conditions for run D, figure 13 shows the distribution of τ_t calculated for each grid box in the model. (As described in §4.2, these calculations start with unit concentration specified in the particular grid box and zero concentration specified elsewhere.) This information is essentially qualitative in so far as the values indicated are a function of the grid size used in the present model (figure 1). Areas of vigorous mixing (τ_t < 10 d), shaded in the figure, can be distinguished from more stagnant regions (τ_t > 20 d). Wherever such contrasting regions are in close proximity creation of thermal fronts is possible, e.g. the Celtic Sea, the north-western Irish Sea and Flamborough Head. Simpson & Hunter (1974)

have shown that the location of such fronts can be linked with a particular value of the parameter H/u_0^3 (u_0 amplitude of the tidal velocity). In the present case τ_t is proportional to $1/\bar{u}$ ($\bar{u}$ residual velocity) for purely advective mixing or $1/K$ (i.e. $1/u_0^2$) for purely dispersive mixing (Zimmerman 1976). For the case of $\bar{u}$ derived directly from Stokes transport, $\bar{u} \propto u_0^2/H$.

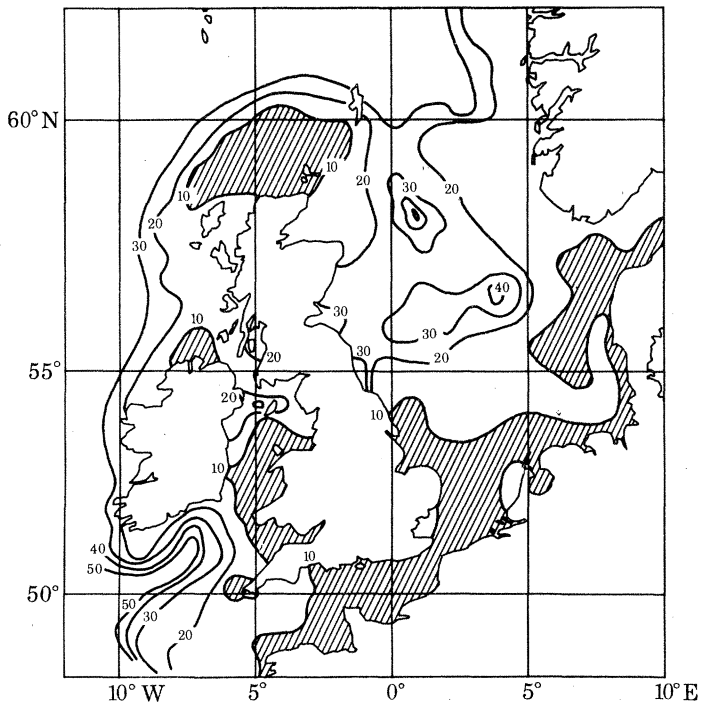

FIGURE 13. 'Turn-over-times' for model grid-boxes in days, grid box size 20′ latitude × 30′ longitude.

Hence for both mixing processes a link with the Simpson–Hunter criterion can be seen. However, the latter criterion introduces more directly the influence of water depth H on the stability of vertical mixing.

4.4. *Age*

Figures 14*a* and *b* show the age distributions of material released (at a constant rate) from Windscale and Cap de la Hague respectively. For Windscale releases travelling in a northerly direction, after 1 year material is centred around Islay; in successive years the centroid reaches the Pentland Firth, Firth of Forth, The Wash and, after 5 years, the Skagerrak. These times are in close agreement with the travel times deduced by Kautsky *et al.* (1980) from observed distributions of ^{137}Cs. After six years, the centroid of material travels beyond the North Sea. For Cap de la Hague releases, corresponding annual milestones are: just beyond the Dover Strait; almost into the Skagerrak; 59° N along the Norwegian Coast; and finally beyond the North Sea after 4 years. The two year travel time to reach the Skagerrak agrees well with model results shown by Maier-Reimer (1977) and with observational data for ^{137}Cs presented by Kautsky (1973).

From (20), figure 15*a* shows the temporal contributions to the parameter τ_a derived for the whole North Sea (i.e. sub-regions 1 to 8 in figure 11). Results are shown for releases from both Windscale and Cap de la Hague. The two curves show initial rises to reach peaks after

1000 and 400 d respectively, these periods correspond to the entry of material to the North Sea. The values $\tau_a = 1560$ d for Windscale releases and 950 d for Cap de la Hague reflect the general pattern of progression noted above from figures 14*a* and *b*.

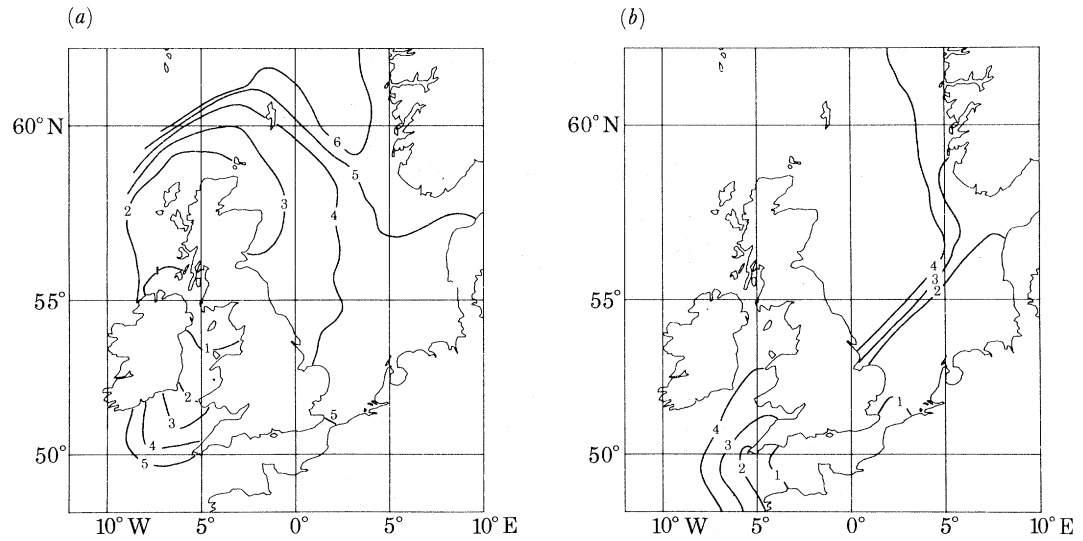

FIGURE 14. (*a*) 'Age' (in years) of material discharged from Windscale.
(*b*) 'Age' (in years) of material discharged from Cap de la Hague.

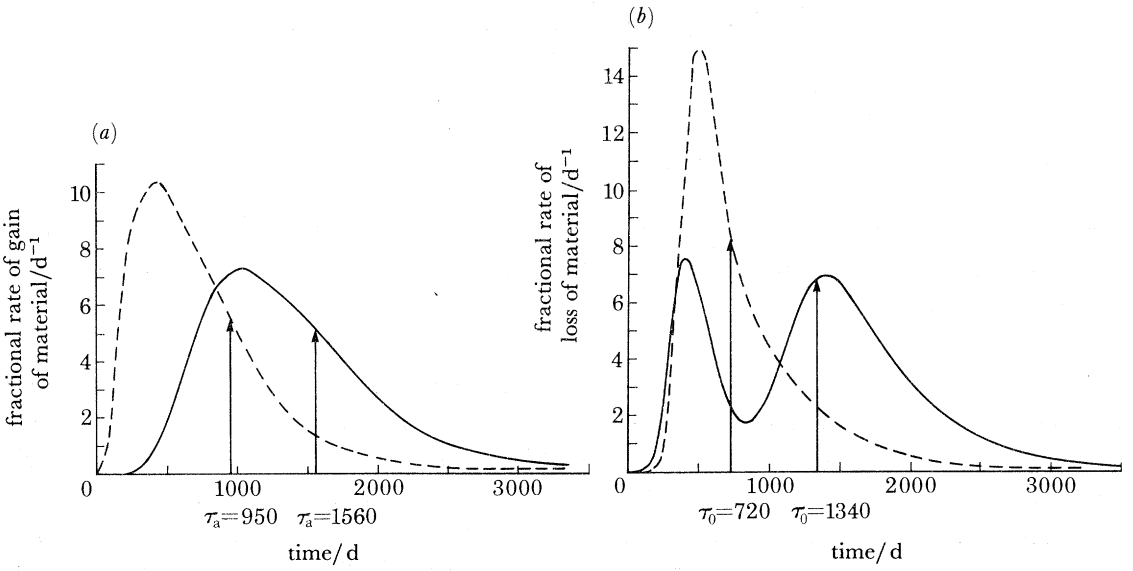

FIGURE 15. (*a*) 'Age' of the North Sea: ——, discharge from Windscale; – – – –, discharge from Cap de la Hague.
(*b*) 'Transit time' for the Continental Shelf: ——, discharge from Windscale; – – – –, discharge from Cap de la Hague.

4.5. *Residence time* τ_r

Figure 16 shows contours of τ_r for the North Sea drawn from discrete values computed for particular grid boxes using the approach outlined in §4.2. Since τ_r reflects the time for material to travel from an initial position to the boundaries of a defined region we note that the present distribution clearly emphasizes the significance of the mean flow pattern shown in figure 5.

Advective transport appears to be the predominant mixing process with values for τ_r increasing with 'travel times' from the Norwegian Shelf outflow region. North Sea residence times could be minimized for U.K. discharges by locating any outflow along the Lincoln or Norfolk coastline.

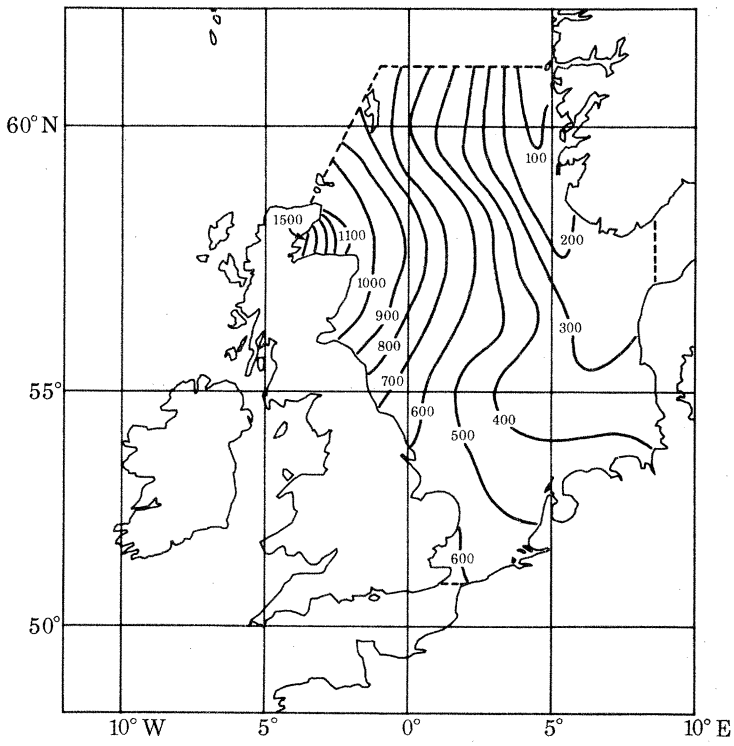

FIGURE 16. 'Residence times' (in days) for the North Sea.

The present values may be compared with corresponding values derived by Maier-Reimer (1979). Overall, the distribution and range of values for τ_r are similar but there are some significant differences. Maier-Reimer shows more structure to the distribution, this may be attributed almost entirely to higher resolution. The calculation of values for figure 16 proved expensive in computing terms and hence values for τ_r were only determined for every fourth grid box, thus Maier-Reimer's results correspond to a linear grid resolution six times greater than the present.

A second major difference is that the present model shows much lower values of τ_r along the coastlines of Belgium, Holland and Germany. In part, this may be attributed to the exclusion of the Skagerrak from the definition of the North Sea region in the present model. The latter region is relatively stagnant in terms of residual flow and thus by including the region within the 'North Sea' material entering from the German Bight would show a higher value of τ_r.

Figure 15*b* shows the temporal contributions associated with the calculation of 'transit times', τ_0, for the complete Shelf region for discharges from both Windscale and Cap de la Hague. (Here the Shelf region is defined as the sea area bounded by the 200 m contour.) Transit time corresponds to residence time when the latter is measured relative to the discharge location and hence these results were calculated with (20) as described in §4.2. The

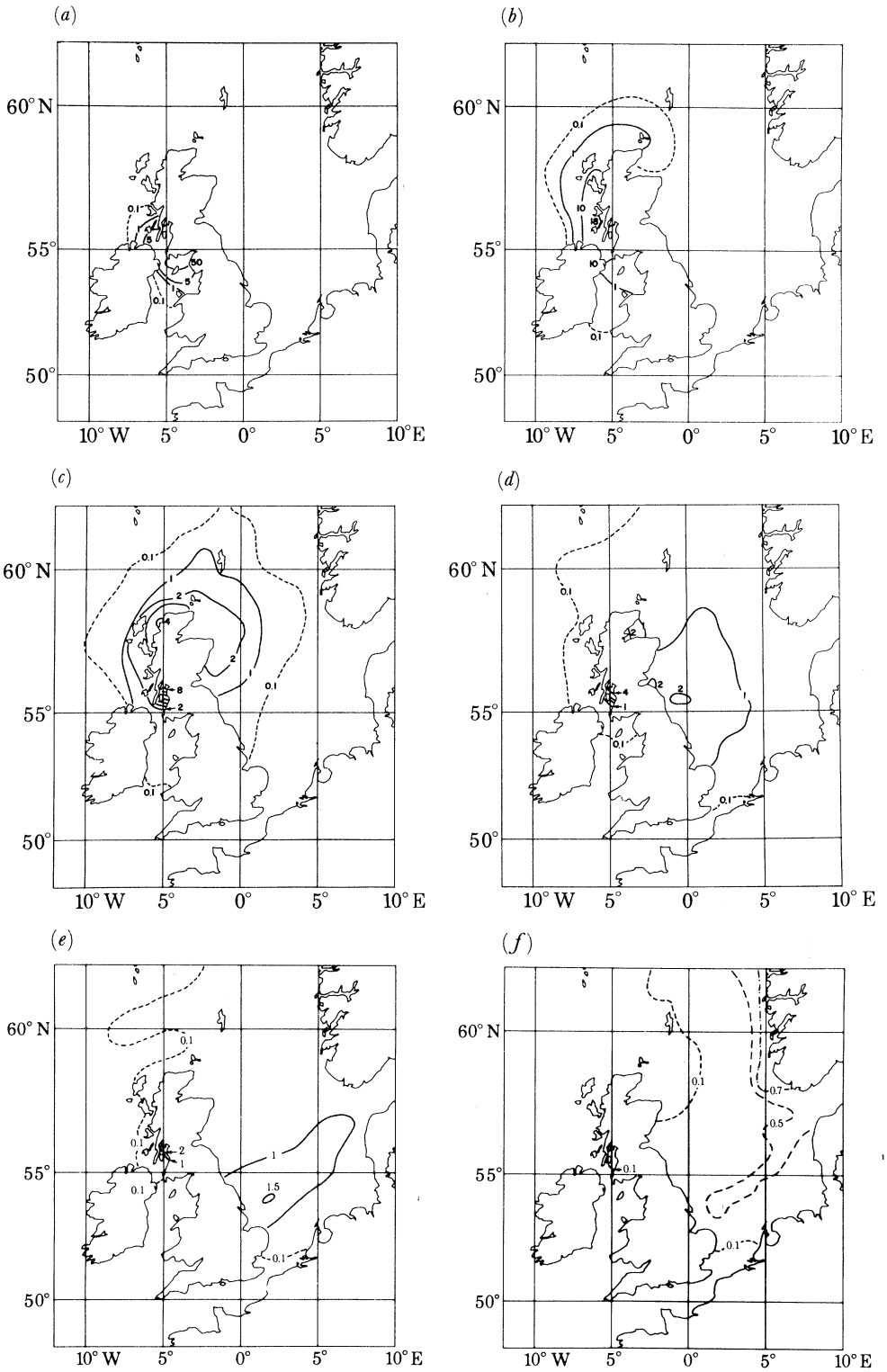

FIGURE 17. Dilution of a single discharge of 10^5 Ci from Windscale. Concentrations in picocuries per litre after (*a*) 60 d; (*b*) 1a; (*c*) 2a; (*d*) 3a; (*e*) 4a and (*f*) 5a.

PHILOSOPHICAL TRANSACTIONS OF THE ROYAL SOCIETY A MATHEMATICAL, PHYSICAL & ENGINEERING SCIENCES

curve for Cap de la Hague follows a predictable pattern with maximum losses of material from the Shelf after 500 d and with a value $\tau_0 = 720$ d. The curve for Windscale exhibits two peaks, it may be deduced that the first peak (after 400 d) corresponds to losses of material along the Shelf edge northwest of Scotland. From the area under the curve between $t = 0$ and the trough at $t = 870$ d it may be estimated that approximately one-third of the material discharged from Windscale is lost in this region. However, earlier model runs showed that dispersion was significant in this region and hence this fraction could be sensitive to the specification of K_x and K_y. The second peak after about 1400 d marks the loss of material in the Norwegian Trench region and thus, overall, $\tau_0 = 1340$.

4.6. *Dilution rates*

The preceding emphasis on time constants omits important results regarding dilution rates. Figures 17*a–f* show a time history of the spread of an instantaneous discharge of 10^5 Ci from Windscale, again with the conditions as specified for run D. After 7.5 years concentrations throughout the model are less than 0.2 pCi l^{-1}. The timing and direction of spreading concur with the patterns established from earlier figures, e.g. 15*a*. However, these later results now enable an estimate to be made of the net concentration at any instant by superimposing distributions related to the time series of past discharges.

5. Summary and conclusions

A two-dimensional numerical model has been formulated to simulate long-term mixing in the coastal waters over the northwest European Continental Shelf. The hydrodynamic section of this model includes a tidal and wind-driven component but density-driven currents were neglected. By locating the open-boundaries of the model in deep water beyond the shelf edge, it was demonstrated that the residual shelf circulation is insensitive to any sea level gradients that might exist in the adjacent oceanic regions.

The tidal component corresponds to the residual circulation extracted from a nonlinear model of the propagation of the predominant M_2 constituent. The wind-driven component is derived by an appropriate summation of the steady-state response of a linearized model to winds from the west and south respectively.

There is a surprising similarity between the circulation patterns associated with these three residual components. This similarity is closest in the deeper areas of the shelf seas and suggests that such flows are close to a geostrophic balance with consequent topographic steering. The validity of the calculated long-term circulation is established by comparison with (i) similar modelling studies, (ii) direct measurements of long-term flows, and (iii) mean sea level variations.

A mixing model was developed from this hydrodynamic model and it is shown that the use, in this model, of residual flow components as opposed to instantaneous currents avoids the problem of excessive numerical dispersion. Optimal values of the turbulent dispersion coefficients were derived by comparison between model simulations of the spread of ^{137}Cs discharged from Windscale and corresponding observational survey data. The determination of these coefficients was the only 'tuning' process used in this study. Sensitivity tests showed that the good agreement shown between model results and observations was not simply a consequence of careful 'tuning'. In many regions advective transport predominated over dispersive

processes, and thus, overall agreement was shown to depend on accurate simulation of both mechanisms.

Observed transport routes were well reproduced both spatially and temporally. At the end of the transport route, i.e. in the Skagerrak and Norwegian coastal region, observed concentrations were reproduced to within about 20%. This accuracy may be viewed against (i) a dilution rate of more than 20 relative to concentrations in the North Channel, and (ii) a total transit time of up to 6 years.

The overall distribution of material within the North Sea is shown to be primarily determined by the pattern of advective transport. This transport is predominantly wind driven. However, since the relevant time-scales for mixing are of the order of years, the distribution of material can be related to the mean wind stress averaged over periods of three months or longer. Thus, the large scale mixing pattern is only indirectly related to the influence of individual storm events.

The accuracy of simulation declined in the later years after 1976 with appreciable divergence originating within the Irish Sea. Model simulation of this region is generally inadequate owing to limited resolution and an examination of the cause of this divergence will require a more detailed model of this region: possibly in three dimensions.

The model was used to determine various time constants for the Shelf seas, e.g. the 'age' of the North Sea for Windscale discharges was calculated as $\tau_a = 1560$ d while for discharges from Cap de la Hague $\tau_a = 950$ d. The turn-over-time of the North Sea was estimated as $\tau_t = 530$ d whereas for the Irish Sea $\tau_t = 328$ d. Values of τ_t were also estimated for sub-regions of the North Sea and these values were found to be within a factor of 2 of related values calculated from a fully three-dimensional hydrodynamic model. A study of residence times showed that about one-third of the material discharged from Windscale is lost to oceanic waters along the Shelf edge northwest of Scotland.

Localized values for τ_t calculated throughout the Shelf Seas distinguish between areas of vigorous mixing and more stagnant regions. Proximity of these regions indicates conditions conducive to the formation of thermal fronts and several such areas appear to correspond with known frontal locations.

A time history of spreading rates for Windscale discharges is presented, this can be used to estimate concentrations for any combination of past discharges.

This study represents a first attempt to simulate the complete mixing process of the Windscale effluent throughout the Shelf seas. We may use this study to address two important questions, one concerning the observation programme and another concerning future modelling efforts. With regard to using observational surveys of ^{137}Cs concentrations for evaluating models of the type described here, valid comparisons require the observational data to be representative of conditions averaged over the same length- and time-scales as used in the model. In surveying from ships, this criterion can best be achieved by avoiding areas where concentrations change rapidly. However, surveying in areas of rapid variation is necessary if synoptic distributions are to be constructed from survey data alone! Present results might be used to determine certain fixed locations (perhaps corresponding to regular increments in 'travel time' from Windscale) where regular sampling could be undertaken. Results presented here would suggest that the sampling intervals should increase with distance from Windscale.

Future modelling efforts could include the use of the existing model to study the mixing of other elements (Livingston *et al.* 1982) or the more general problem of the prediction of

temperature and salinity distributions. While the accuracy of simulation achieved with the present model exceeded initial expectations, ultimately more sophisticated models must be employed with improved spatial and temporal resolution including fully three-dimensional hydrodynamics, density effects and freshwater inflows. Possibly, such models could be linked to atmospheric and oceanic models to provide real-time forecasting of water quality parameters in similar fashion to the existing U.K. surge prediction model. Updating of this model could be carried out with various data derived from satellite surveillance. Whether such developments are worthwhile is difficult to judge, obvious benefits would include forecasting of fog formation and fisheries advice. Undoubtedly, many additional unforseen benefits could accrue.

The work described in this paper was funded by the Natural Environment Research Council and by the Ministry of Agriculture, Fisheries and Food. The author is indebted to a number of colleagues from I.O.S. Bidston, in particular to R. Flather for providing tidal data, N. S. Heaps for comments on the manuscript, K. R. Thompson for providing wind data and R. Smith for drafting work. D. F. Jefferies of M.A.F.F., Lowestoft supplied much useful information relating to the ^{137}Cs distributions.

References

Ancellin, J. & Bovard, P. 1980 *Proceedings of the 3rd NEA Seminar on Marine Radioecology*, Tokyo 1979. Paris: O.E.C.D.
Bolin, B. & Rodhe, H. 1973 *Tellus* **25**, 58–62.
Boris, J. P. & Book, D. L. 1973 *J. Comput. Phys.* **11**, 38–69.
Bowden, K. F. 1950 *Mon. Not. R. astr. Soc. geophys. Suppl.* **6**, 63–90.
Bowden, K. F. & Hughes, P. 1961 *Geophys. Jl R. astr. Soc.* **5**, 265–291.
Cartwright, D. E., Edden, A. C., Spencer, R. & Vassie, J. M. 1980 *Phil. Trans. R. Soc.* A, **298**, 87–139.
Davies, A. M. 1980 *Met. ForschErgebn.* A **22**, 53–68.
Davies, A. M. 1982 *Oceanologica Acta* **5** (3), 269–279.
Davies, A. M. & Heaps, N. S. 1980 *Tellus* **32**, 164–175.
Dooley, H. D. 1974 *J. Cons. perm. int. Explor. Mer.* **36**, 54–61.
Fischer, H. B., List, E. J., Koh, R. C. Y., Imberger, J. & Brooks, N. H. 1979 *Mixing in inland and coastal waters.* New York: Academic Press.
Heaps, N. S. 1969 *Phil. Trans. R. Soc.* A **265**, 93–137.
Heaps, N. S. 1978 *Dt. hydrogr. Z.* **31**, 147–169.
Howarth, M. J. 1982 In *Hydrodynamics of semi-enclosed seas* (ed. J. C. J. Nihoul), pp. 205–242. Amsterdam: Elsevier.
I.C.E.S. 1970 *Monthly means of surface temperature and salinity for areas of the North Sea and North-eastern North Atlantic.* Copenhagen: International Council for the Exploration of the Sea.
I.C.E.S. 1983 *Report of I.C.E.S. Study Group on the Flushing Times of the North Sea.* Co-operative Research Report 123.
Jefferies, D. F., Steele, A. K. & Preston, A. 1982 *Deep Sea Res.* A **29**, 713–738.
Kautsky, H. 1973 *Dt. hydrogr. Z.* **26**, 241–246.
Kautsky, H. 1976 *Dt. hydrogr. Z.* **29**, 217–221.
Kautsky, H., Jefferies, D. F. & Steele, A. K. 1980 *Dt. hydrogr. Z.* **33**, 152–157.
Lee, A. J. & Ramster, J. W. (eds) 1981 *Atlas of the seas around the British Isles.* Ministry of Agriculture, Fisheries and Food, Directorate of Fisheries Research.
Livingston, H. D., Bowen, V. T. & Kupferman, S. L. 1982 *J. mar. Res.* **40**, 1227–1258.
Maier-Reimer, E. 1977 *Dt. hydrogr. Z.* **30**, 69–80.
Maier-Reimer, E. 1979 *Dt. hydrogr. Z.* **32**, 126–130.
McKinley, I. G., Baxter, M. S., Ellett, D. J. & Jack, W. 1981 *Estuar. coast. mar. Sci.* **13**, 69–82.
Oerlemans, J. 1978 *Dt. hydrogr. Z.* **31**, 182–189.
Pingree, R. D. & Griffiths, D. K. 1980 *Oceanologica Acta* **3** (2), 227–236.
Prandle, D. 1974 Institute of Oceanographic Sciences, Rep. no. 4, 25 pp. (unpublished manuscript).
Prandle, D. 1978 *Proc. R. Soc. Lond.* A **359**, 189–228.
Roache, P. J. 1976 *Computational fluid dynamics.* Albuquerque, N. M.: Hermosa.
Rossiter, J. R. 1967 *Geophys. Jl R. astr. Soc.* **12**, 259–299.
Simpson, J. H. & Hunter, J. R. 1974 *Nature, Lond.* **250**, 404–406.

PHILOSOPHICAL TRANSACTIONS OF THE ROYAL SOCIETY A MATHEMATICAL, PHYSICAL & ENGINEERING SCIENCES

Thompson, K. R., Marsden, R. F. & Wright, D. G. 1983 *J. phys. Oceanogr.* **13**, 1003–1011.
Wang, D. P. 1982 *J. phys. Oceanogr.* **12**, 1524–1526.
Zalesak, S. T. 1979 *J. Comput. Phys.* **31**, 335–362.
Zimmerman, J. T. F. 1976 *Neth. J. Sea Res.* **10**, 149–191.
Zimmerman, J. T. F. 1981 *Nature, Lond.* **290**, 549–555.

PHILOSOPHICAL TRANSACTIONS OF THE ROYAL SOCIETY A MATHEMATICAL, PHYSICAL & ENGINEERING SCIENCES